# Computationally Efficient Skew Effect Calculation in Electric Machines Utilising Harmonic Maxwellian Stress Decomposition

C. M. Spargo, B. C. Mecrow and J. D. Widmer

***Abstract* – A novel finite element solution post-processing technique to determine the effects of rotor skewing is presented in this paper. It was previously proposed that a post-processing semi-numerical method to calculate the harmonic torque components in synchronous machines is useful to machine designers. Harmonic Maxwellian stress components create parasitic effects during machine operation such as torque ripple, which is extremely undesirable in many applications and is a major cause of acoustic noise and vibration which can limit the machine's application. Rotor skewing usually allows reduction of this torque ripple and this paper expands previous work to include a good approximation of skewing effects using a single 2D time stepping Finite Element (FE) study with the developed post-processing method. The method reduces computation time for skew effect calculation where a large 3D FE simulation would usually be required.**

***Index Terms*—Electric motor, Maxwell stress tensor, harmonics, skew, synchronous machines, torque ripple.**

## I. Introduction

HARMONIC content in the airgap of electrical machines is inherent due to the non-ideal nature of the machine's geometry and excitation. Torque ripple is a major concern in electrical machines causing unwanted acoustic vibration and noise [1] as well as inducing potential mechanical damage to the machine's insulation system [2]. This parasitic effect can also limit the machine's application range, for example military and aerospace applications where low noise and vibration are required. Effective reduction of these parasitic effects is an important consideration and challenge for electrical machine designers, though few analysis tools give helpful information into the causes. Finite element analysis alone only predicts the total instantaneous rotor electromagnetic torque. It has been shown previously [3] that post-processing is required. In terms of torque ripple, no information relating to the composition can be explicitly found when using conventional techniques, only the resultant torque waveform, with calculations of mean torque and torque ripple as a percentage are available. Fractional slot concentrated windings (FSCW) bring many advantages to the design of synchronous machines [4], however in machines with fractional slot concentrated windings the space harmonic content in the airgap is greater than a distributed winding. Therefore, the magnitude of these parasitic effects are greater and consequently the importance of their analysis and minimization is increased. The space harmonic content derives from the winding factors of particular winding patterns, which depends upon the machine slot-pole combinations [4]. Space harmonic analysis of FSCW MMF waves and analysis of their effects on permanent magnet synchronous machines (PMSM) performance is detailed in [5] and in synchronous reluctance machines [4]. The space harmonics cause perturbations in the Maxwell Stress tensor, leading to high torque ripple. The aim of the paper is to extend the previously published semi-numerical post-processing technique [3] for efficient computation of the effect of skew in synchronous machines in relation to the previously designed cSynRM. The machine originally exhibited high torque ripple, but was reduced through improved electromagnetic design, however rotor skew could also be used [6] at the expense of mean torque. The developed technique eliminates computationally intensive 3D finite element solutions and reduces the computation to a 2D finite element calculation with a quick post-processing computation and gives insights previously unobtainable.

## II. Maxwell Stress Tensor

The Maxwell stress tensor $\bar{\bar{T}}$ [7] is extensively used in the calculation of forces and torques in electric machines [8], (in space $\mathbb{R}^2$ with cylindrical coordinates);

$$\bar{\bar{T}} = \frac{1}{\mu_0}\begin{bmatrix} \dfrac{B_r^2 - B_\theta^2}{2} & B_r B_\theta \\ B_\theta B_r & \dfrac{B_\theta^2 - B_r^2}{2} \end{bmatrix} \tag{1}$$

The rotor force density can be shown to be expressed as a surface integral;

$$\mathbf{F} = \oiint_{\partial S} \bar{\bar{T}} \cdot d\mathbf{S} \tag{2}$$

In the tensor matrix, elements $a_{11}$ and $a_{21}$ are the radial magnetic pressure and the tangential shear stress acting upon the rotor surface $S_1$, depicted in Fig. 1. The former is linked to

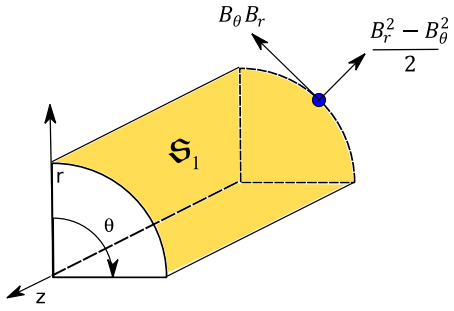


Fig. 1. Rotor surface, $S_1$, on which the Maxwell stress tensor acts. Torque production is tangential to the surface and the radial force density is normal to the surface.

The authors are with the Power Electronics, Drives and Machines Research Group, School of Electrical and Electronic Engineering, Newcastle University, UK. Corresponding author: c. m. spargo (e-mail: c.m.spargo@ncl.ac.uk).

magnetic pull and the latter determines the torque production in the machine and also the torque ripple [3].

## III. Airgap Field

In general, the airgap field of an electrical machine can be expressed;

$$B(\theta) = \sum_{v}^{\infty} |B_v| \Re e\{e^{iv\theta + i\widehat{\varphi_v}}\} \tag{3}$$

Time stepping finite element analysis provides access to accurate airgap fields at the desired machine operating points. Extraction of the air gap field defined by an arc in the centre of the air gap is then performed through post-processing. The airgap flux density can be discretised and extracted;

$$\mathbf{B}[\theta, t] = B_\theta[\theta, t] + jB_r\,[\theta, t] \tag{4}$$

where $B_\theta$ and $B_r$ are the tangential and radial magnetic flux density components around the airgap circumference as a discrete function of time and space respectively. The angle around the airgap is discretised according to;

$$\theta = n\left(\frac{2\pi}{N}\right);\ n \in \mathbb{Z} : 0 \le n \le N \tag{5}$$

where *n* is the discrete sample index and *N* is the number of samples. The radial and tangential components, around the air gap at each point in time can then be decomposed into harmonics, *v*, using a discrete space Fourier series;

$$B[v] = \frac{1}{N}\sum_{n=0}^{N-1} |B[\theta]|\, e^{-ivn\left(\frac{2\pi}{N}\right)} \in \mathbb{C} \tag{6}$$

It can be shown that the inverse transform of Eq. (6) can be represented;

$$B[\theta] = 2\sum_{v=1}^{\frac{N-2}{2}} \Re e\left\{|B[v]| e^{i\left(v\theta + \widehat{\varphi_{\theta v}}\right)}\right\} \in \mathbb{R} \tag{7}$$

Evaluation of the field around the air gap at each time instant is performed to obtain the magnetic field used for subsequent post-processing calculations of the harmonic quantities. The term $\Omega_0 = \frac{2\pi}{N}$ is the discrete angle. These transforms allow calculation of the radial and tangential fields at a point in time (or specific rotor angle) as;

$$B_r[\theta] = 2\sum_{v=1}^{\frac{N-2}{2}} |B_r[v]| \Re e\left\{e^{iv\Omega_0\theta}\right\} \tag{8}$$

$$B_\theta[\theta] = 2\sum_{v=1}^{\frac{N-2}{2}} |B_\theta[v]| \Re e\left\{e^{iv\Omega_0\theta}\right\} \tag{9}$$

The tangential and radial field components are transformed from the global *x-y* coordinate system into the local cylindrical coordinate system by a linear transformation;

$$\begin{bmatrix} B_r \\ B_\theta \end{bmatrix} = \begin{bmatrix} -\sin(\theta) & \cos(\theta) \\ \cos(\theta) & \sin(\theta) \end{bmatrix} \cdot \begin{bmatrix} B_x \\ B_y \end{bmatrix} \tag{10}$$

The parameters $B_x$ and $B_y$ must be predetermined for all airgap angles and rotor positions for the semi-numerical analysis to work through population of the field values into the developed equations. Where the field functions can be written in the continuous domain;

$$B_r(\theta) = 2\sum_{v=1}^{\infty} |B_{rv}|\, \Re e\left\{e^{i\left(v\theta + \widehat{\varphi_{rv}}\right)}\right\} \tag{11}$$

$$B_\theta(\theta) = 2\sum_{v=1}^{\infty} |B_{\theta v}| \Re e\left\{e^{i\left(v\theta + \widehat{\varphi_{\theta v}}\right)}\right\} \tag{12}$$

These expressions are then used to calculate the rotor electromagnetic torque. However, they must be modified in order to account for slot skewing on the rotor or stator.

## IV. Incorporation of Skew

In electric machine modelling, skew requires a 3D finite element computation which is time consuming. A quick method to assess the effect of skewing on torque quality would be useful to machine designers. In developing a mathematical model of skew effect prediction using only faster 2D finite element solutions, the harmonic skew factor is useful [9];

$$k_{skv} = \mathrm{sinc}\left(\frac{vp\pi\theta_m^{\deg}}{360}\right) = \frac{360}{vp\pi\theta_m^{\deg}} \sin\left(\frac{vp\pi\theta_m^{\deg}}{360}\right) \tag{13}$$

where $\theta_m^{\deg}$ is the skew angle in mechanical degrees and *p* the number of rotor poles. The airgap flux density is proportional to the resultant MMF, which is a rotating wave in space and time that can be decomposed into harmonic contra-rotating MMF waves, the MMF is written;

$$F_m(\theta, t) = \sum_{v=1}^{\infty}\sum_{c=1}^{n_c} \frac{4N\xi_v}{vp\pi}\{F_{mv}^{+}(\theta, t) + F_{mv}^{-}(\theta, t)\} \tag{14}$$

Forwards $F_{mv}^{+}$ and backwards $F_{mv}^{-}$ rotating harmonic MMF components can be written as co-sinusoidal functions in space and time. The term $\xi_v$ is the winding factor incorporating the skew factor, $k_{skv}$ as $\xi_v = k_{skv}k_{dv}k_{pv}$ where $k_{dv}$ is the distribution factor and $k_{pv}$ is the pitch factor. In the previous analysis [3], the pitch and distribution factors are taken into account, however the skew factor can be considered in post processing. We can write that;

$$B(\theta, t) \propto F(\theta, t)\Lambda^{-1}(\theta) \tag{15}$$

where $\Lambda^{-1}(\theta)$ is the inverse airgap permeance function, where it can be shown that [10];

$$\Lambda^{-1}(\theta) = \frac{\mu_0}{k_C g}\left(1 + \sum_{v=1}^{\infty} A_v \cos(v\theta Q_s)\right) \tag{16}$$

$k_C$ is the Carter coefficient, $g$ the minimum airgap length and $Q_s$ the number of stator slots. The relative value of the harmonic permeance holds the following relation;

$$A_v \propto k_{skv} \tag{17}$$

Consequently;

$$B(\theta,t) \propto k_{skv}^2 \tag{18}$$

Therefore, equations 11 and 12 can then be modified to allow for closed form prediction of skewing;

$$B_r(\theta) = 2\sum_{v=1}^{\infty} k_{skv}^2 |B_{rv}|\, \Re e\left\{e^{i(v\theta+\widehat{\varphi_{rv}})}\right\} \tag{19}$$

$$B_\theta(\theta) = 2\sum_{v=1}^{\infty} k_{skv}^2 |B_{\theta v}| \Re e\left\{e^{i(v\theta+\widehat{\varphi_{\theta v}})}\right\} \tag{20}$$

It is then possible to continue the analytical analysis so that post-processing of finite element studies can yield approximations of the rotor skewing effect without the requirement of computationally intensive 3D finite element models.

## V. Closed-Form Theory of Tangential Force

In developing equations relating to the electromagnetic torque production, the tangential shear stress element of the Maxwell Stress Tensor is the quantity of interest;

$$\sigma_\theta(\theta,t) = \frac{B_\theta(\theta,t)B_r(\theta,t)}{\mu_0} = \frac{1}{\mu_0}\sum_{v=1}^{\infty} B_{\theta v}(\theta,t)B_{rv}(\theta,t) \tag{21}$$

with the corresponding torque calculated by;

$$T_\theta(t) = r^2 \int_0^{l_a}\int_0^{2\pi} \sigma_\theta(\theta,t)\, d\theta dz \tag{22}$$

These expressions yield only the resultant shear stress and electromagnetic torque. Modifying Eq. 21 by incorporating skew factor;

$$\sigma_\theta(\theta,t) = \frac{k_{skv}^4}{\mu_0}\sum_{v=1}^{\infty} B_{\theta v}(\theta,t)B_{rv}(\theta,t) \tag{23}$$

Eq. 23 yields a closed loop solution and enables access to the harmonic torque components due to individual field harmonics incorporating skew effects. The rotor shear stress equation must be written for a point in time;

$$\sigma_{\theta v} = \left(\frac{4|B_{\theta v}||B_{rv}|}{k_{skv}^{-4}\mu_0}\right)\Re e\left\{e^{i(v\theta+\widehat{\varphi_{\theta v}})}\right\}\Re e\left\{e^{i(v\theta+\widehat{\varphi_{rv}})}\right\} \tag{24}$$

Setting for convenience $\widehat{\varphi_{rv}} = 0$ and defining $\varphi_{dv} \triangleq \widehat{\varphi_{\theta v}} - \widehat{\varphi_{rv}}$, an equation for electromagnetic torque for an individual field harmonic order is;

$$T_{\theta v} = \mathcal{M}\int_0^{2\pi} \Re e\left\{e^{i(v\theta+\widehat{\varphi_{dv}})}\right\}\Re e\left\{e^{iv\theta}\right\} d\theta \tag{25}$$

Where;

$$\mathcal{M} = \frac{4k_{skv}^4|B_{\theta v}||B_{rv}|r^2 l_a}{\mu_0} \tag{26}$$

This integral is non-trivial and cumbersome in exponential form and is best performed by transforming the exponentials into trigonometric functions;

$$\frac{T_{\theta v}}{\mathcal{M}} = \frac{\sin(2v\theta+\varphi_{dv}) + 2v\theta\cos(\varphi_{dv})}{4v}\Bigg|_{\theta=0}^{\theta=2\pi} = \left(\frac{\sin(4\pi v+\varphi_{dv}) - \sin(\varphi_{dv})}{4v} + \pi\cos(\varphi_{dv})\right) \tag{27}$$

By analysis, for $v \in \mathbb{Z} \Rightarrow \sin(4\pi v+\varphi_{dv}) \to \sin(\varphi_{dv})$, thus the first term in eq. (27) disappears and the harmonic torque equation is now a relatively simple equation;

$$T_{\theta v} = \left(\frac{4\pi k_{skv}^4 l_a r^2 |B_{rv}||B_{\theta v}|}{\mu_0}\right)\Re e\{e^{i\varphi_{dv}}\} \tag{28}$$

The total torque at a time instant due to all harmonics is readily calculated as;

$$T_\theta = \left(\frac{4\pi k_{skv}^4 l_a r^2}{\mu_0}\right)\sum_{v=1}^{\infty}|B_{rv}||B_{\theta v}|\,\Re e\{e^{i\varphi_{dv}}\} \tag{29}$$

Therefore it is now possible to obtain information relating to the actual contribution of each field harmonic to the torque waveform and consequently the torque ripple. This information was previously unobtainable. Noting that $\pi l_a r^2 = V_r$ the rotor electromagnetic volume;

$$T_{\theta v} = \left(\frac{4V_r k_{skv}^4}{\mu_0}\right)|B_{rv}||B_{\theta v}|\,\Re e\{e^{i\varphi_{dv}}\} \tag{30}$$

which for the total torque at a time instant;

$$T_\theta = \left(\frac{4V_r}{\mu_0}\right)\sum_{v=1}^{\infty} k_{skv}^4|B_{rv}||B_{\theta v}|\,\Re e\{e^{i\varphi_{dv}}\} = \left(\frac{4V_r}{\mu_0}\right)\sum_{v=1}^{\infty} k_{skv}^4|B_{rv}||B_{\theta v}|\cos\varphi_{dv} \tag{31}$$

The full expression for a particular time instant is therefore;

$$T_\theta = \mathcal{L}\sum_{v=1}^{\infty}|B_{rv}||B_{\theta v}|\cos(\varphi_{dv})\sin^4\left(\frac{vp\theta_m^{\mathrm{rad}}}{2}\right) \tag{32}$$

where

$$\mathcal{L} = \left(\frac{64V_r}{\mu_0}\right)\left(vp\theta_m^{\mathrm{rad}}\right)^4 \tag{33}$$

This allows an approximate prediction of how a skew angle $\alpha$ affects the torque quality in the machine. Usually this is not

possible to implement as access to individual torque components is not available. The skew factor (a cardinal sinusoidal function) is presented in Fig. 4. This analysis assumes that the skewing is uniform along the machine length and no 'stepped skewing' is used. To revert to an unskewed machine, $k_{skv}^4 = 1 \forall v$ in (31).

## VI. Implementation

Easy implementation of the derived equations is possible through post-processing of a 2D finite element solution and designing a MATLAB script to facilitate this post processing. A simplified block diagram of implementation is presented in Fig. 2.

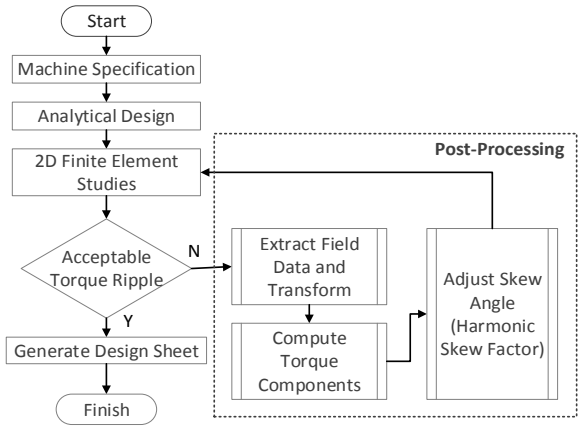


Fig. 2. Implementation of the developed method

A 2D finite element time stepping model must be solved initially – the airgap fields are then extracted and transformed in MATLAB. From these fields the harmonic torque components (for each time instant) without skew effects are calculated and then scaled based on calculated skew factors for the correct skew angle and machine slot-pole combination, according to Eq. 30. The torque harmonics are then summed over the entire range to obtain the resultant torque waveform with the effects of rotor skew, this provides an estimate of the torque waveform with a skewed rotor from 2D FEA.

## VII. Application

In order to compare the developed technique based on Eq. 32 and 3D finite element analysis, the 6 slot 4 pole synchronous reluctance motor that is known to exhibit torque ripple is analysed and results compared. The machine has a 150mm outer diameter and stack length with a 0.5mm airgap. The rated torque with an unskewed rotor is 20Nm at 1500rpm. The torque ripple is approximately 40% of the mean torque with the unskewed rotor where mean torque and torque ripple are respectively calculated;

$$T_\theta^{\text{mean}} = \frac{1}{N-1}\sum_{t=0}^{T} T_\theta^t \tag{34}$$

$$T_\theta^{\%\text{av}} = \frac{\max(T_\theta^{\forall t}) - \min(T_\theta^{\forall t})}{T_\theta^{\text{mean}}} \tag{35}$$

$T_\theta^t$ is the torque at time $t$ and $T$ is the end time of the cycle. The rotor is skewed up to 60 mechanical degrees which equates to one stator slot pitch. Figure. 3 shows the unskewed rotor with rotors skewed at 30 and 60 degrees. Figure. 4 shows the skew factors for the 4 pole machine with skew angle in mechanical degrees. Figure 5 shows the relative reduction in torque magnitude with skew angle based on Eq. 30.

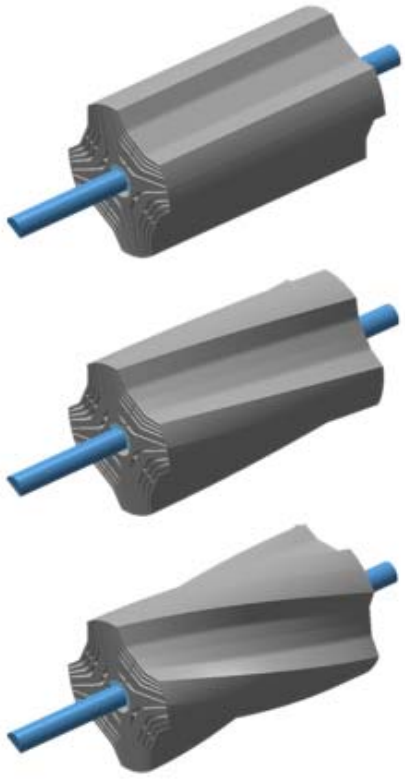

Fig. 3. Top: Unskewed; Middle: 30 degrees skew; Bottom: 60 degrees skew.

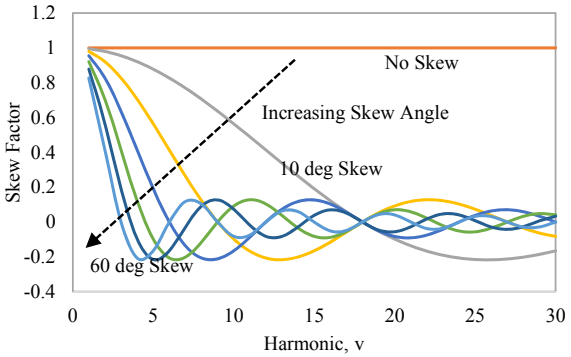


Fig. 4. Harmonic skew factors with skew angle.

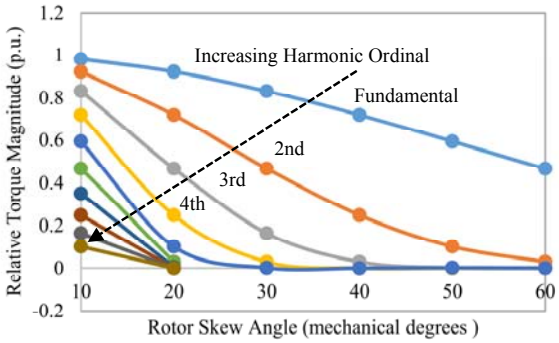


Fig. 5. Harmonic skew factors with skew angle.

Through 2D finite element time stepping studies and the developed post processing method, the torque with no rotor skew was reconstructed from the torque harmonic components, presented in Fig. 6. The waveform match is reasonably good with the vast majority of content replicated. Figure 7 presents a comparison of the waveforms between the 3D FEA and the 2D FEA + post processing with 30 degrees

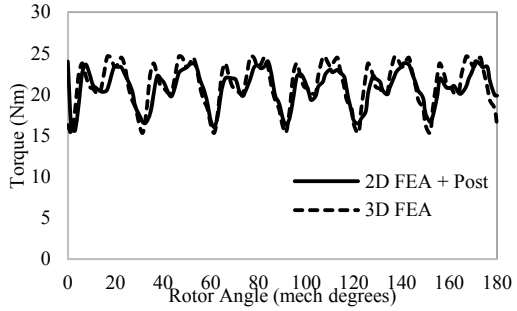


Fig. 6. Torque profile of unskewed rotor.

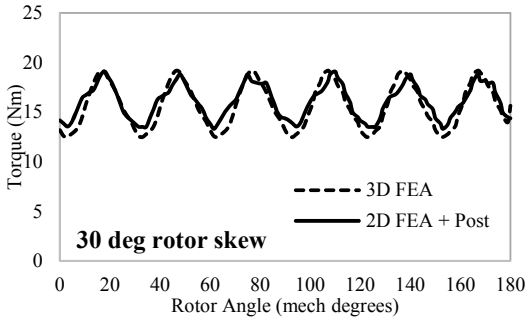


Fig. 7. Torque profiles with 30 degree rotor skew.

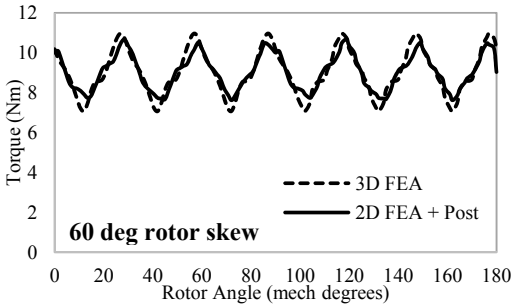


Fig. 8. Torque profiles with 60 degree rotor skew.

of rotor skew. Figure 8 presents the comparison at 60 degrees rotor skew. Table I presents a summary of results..

TABLE I
3D FEA VS 2D FEA WITH POST PROCESSING

| Skew Angle (deg) | 3D FEA | | 2D FEA w/POST | |
|---|---|---|---|---|
| | Mean Torque (Nm) | Torque Ripple (% Average) | Mean Torque (Nm) | Torque Ripple (% Average) |
| No Skew | 19.72 | 79.03% | 20.1 *(+2.03 %)* | 44.5% *(-43.69 %)* |
| 30 | 15.66 | 42.78% | 16.05 *(+2.29 %)* | 36.0% *(-15.89 %)* |
| 60 | 9.03 | 43.01% | 9.03 *(+0 %)* | 33.69% *(-21.66%)* |

The results show a good replication of the torque waveform from no skew to 60 degrees skew with a very good match on mean torque, however the accuracy of the torque ripple calculation is limited. The torque ripple is calculated here;

$$\Delta T = \frac{T_{max} - T_{min}}{T_{ave}} \times 100\% \qquad (36)$$

In terms of reducing the torque ripple in the machine, in this case the reduction in mean torque is significant and skew is not warranted. However, the method can be applied to other machines, where the physical insight given by calculating the individual torque contributions for each field harmonic and how their contribution changes with skew could be extremely valuable.

## VIII. COMPUTATION TIMES

It is well known that 3D FEA is a computationally intensive and can take a very long time to solve depending upon the geometry and the mesh size. Two dimensional studies cannot conventionally take into account skew, though solve much faster due to a much smaller number of elements. In this study, the 2D FEA was performed with a fine mesh in the airgap region with a coarser mesh in the less crucial regions (16,936 triangles) – an unskewed 2D FEA took approximately 4 minutes on Intel i7 870, 2.93GHz machine with 16GB of RAM. The 2D FEA post processing takes less than 1 minute, so the combined time for 2D FEA + Post processing is approximately 5 minutes.

As for the 3D FEA, an average solution time with a skewed rotor was 3.5 hours (540,723 tetrahedrons). Therefore the computation time by utilizing 2D FEA with post-processing is significantly reduced (by 97.5%), at the cost of accuracy. The discrepancy in accuracy between the methods is briefly discussed in the next section. A close up of the airgap and surrounding mesh are found in Fig. 9 and the 3D mesh as a whole in Fig. 10.

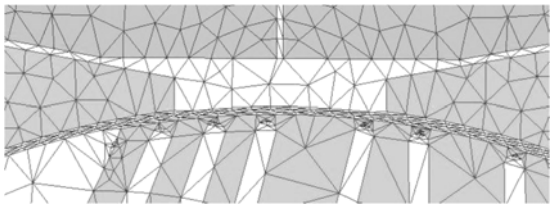

Fig. 9. 2D FEA mesh in the airgap and slot opening.

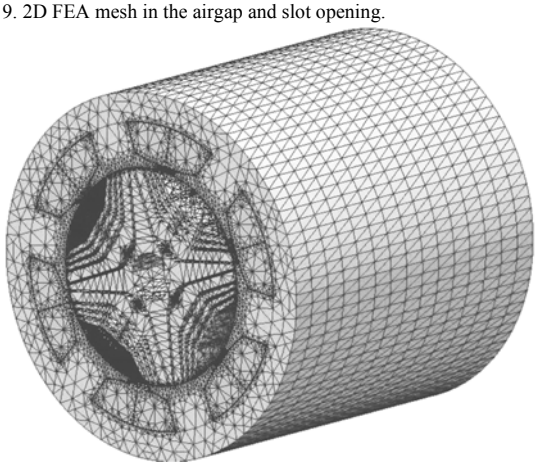

Fig. 10. 3D FEA model mesh.

## IX. Accuracy

The mean torque prediction is consistently within 3% of the 3D FEA solutions however the torque ripple calculation differs significantly due to the variation between the 2D FEA and 3D FEA. This discrepancy not due to the inaccuracy of the method as there is a large difference in the unskewed torque ripple figures. This suggests that the FEA software computes the Maxwell stress tensor using a different method than in Equation 22. In using this method, sensitivity to local field errors is high (which are a distinct possibility) and thus the computed stress tensor is sometimes inaccurate. It is beyond the scope of this paper to consider the optimal evaluation of the Maxwell stress tensor, however it is suggested that to improve the results of this post-processing method, in the case of 2D FEA, a method based on a surface integral over the entire airgap to average the forces would be advantageous. Such a method is described in [11].

## X. Conclusion

This paper has presented a novel 2D finite element post processing method to obtain harmonic torque components based on harmonic decomposition of the Maxwell stress tensor. These harmonic torque components are used to then calculate the effect of rotor skewing by taking into account the effect of the skew factor on the airgap fields and the corresponding Maxwellian stress. It is shown that computation time for traditional 3D FEA skew analysis can be reduced by over 97% by using 2D FEA plus the novel post processing algorithm. The waveform results of the 2D plus post processing match closely to the 3D FEA however due to the method used to evaluate the Maxwell stress tensor, inaccuracies occur. The mean torque calculation is within 3% but a large variation in torque ripple is observed – improvements can be made through advancements in the stress tensor evaluation algorithm.

## XI. References


[1] Eason, Hong-Seok Ko; Kwang-Joon Kim, "Characterization of noise and vibration sources in interior permanent-magnet brushless DC motors," *Magnetics, IEEE Transactions on* , vol.40, no.6, pp.3482,3489, Nov. 2004.

[2] G. Stone, et al, Electrical Insulation for Rotating Machines: Design, Evaluation, Aging, Testing and Repair, IEEE Press Series on Power Engineering, 2004

[3] Spargo, C.M.; Mecrow, B.; Widmer, J., "A Semi-Numerical Finite Element Post-Processing Torque Ripple Analysis Technique for Synchronous Electric Machines Utilizing The Airgap Maxwell Stress Tensor," *Magnetics, IEEE Transactions on* , vol.PP, no.99, pp.1,1

[4] Spargo, C.M.; Mecrow, B.C.; Widmer, J.D., "Application of fractional slot concentrated windings to synchronous reluctance machines," *Electric Machines & Drives Conference (IEMDC), 2013 IEEE International* , vol., no., pp.618,625, 12-15 May 2013

[5] EL-Refaie, A.M.; , "Fractional-Slot Concentrated-Windings Synchronous Permanent Magnet Machines: Opportunities and Challenges," Industrial Electronics, IEEE Transactions on , vol.57, no.1, pp.107-121, Jan. 2010

[6] Alhamadi, M.A.; Demerdash, N.A., "Modeling and experimental verification of the performance of a skew mounted permanent magnet brushless DC motor drive with parameters computed from 3D-FE magnetic field solutions," *Energy Conversion, IEEE Transactions on* , vol.9, no.1, pp.26,35, Mar 1994

[7] Griffiths, David J. *Introduction to electrodynamics*. Pearson, 2013.

[8] Meessen, K. J.; Paulides, J. J H; Lomonova, E. A., "Force Calculations in 3-D Cylindrical Structures Using Fourier Analysis and the Maxwell Stress Tensor," *Magnetics, IEEE Transactions on* , vol.49, no.1, pp.536,545, Jan. 2013

[9] Juha Pyrhonen, et al, Design of Rotating Electrical Machines, 2nd Edition, Wiley, 2013

[10] Jacek F. Gieras, et al, Noise of Polyphase Electric Motors, CRC Press, 2005

[11] McFee, S.; Webb, J.P.; Lowther, D.A., "A tunable volume integration formulation for force calculation in finite-element based computational magnetostatics," *Magnetics, IEEE Transactions on* , vol.24, no.1, pp.439,442, Jan 1988



**Christopher. M. Spargo** received the BEng (Hons) degree in Electrical and Electronic Engineering from the University of Newcastle upon Tyne, Newcastle upon Tyne, U.K. in 2011. He is currently pursuing the Ph.D. degree in the Power Electronics, Machines and Drives research group at the same university in the School of Electrical and Electronic Engineering. He is a past Electrical Energy Engineering Academy Scholar and was awarded the Institution of Engineering and Technology Postgraduate Scholarship in 2011. His research interests include the design, modelling and control of synchronous reluctance machines, applied mathematics and electromagnetic theory. He is actively involved with the Institution of Engineering and Technology, UK and is an associate member of the Institution of Mathematics and its Applications.

**Barrie C. Mecrow** received the Ph.D. degree from the University of Newcastle upon Tyne, Newcastle upon Tyne, U.K., for his research into 3-D eddy-current computation applied to turbogenerators. He commenced his career as a Turbogenerator Design Engineer with NEI Parsons, Newcastle upon Tyne, U.K. He became a Lecturer in 1987 and a Professor in 1998 with Newcastle University, Newcastle upon Tyne. He is the Head of the School of Electrical and Electronic Engineering, Newcastle University, where he is also a Professor of electrical power engineering. His research interests include fault-tolerant drives, high-performance permanent-magnet machines, and novel switched reluctance drives. He is actively involved with industry in the aerospace, automotive, and consumer product sectors, who fund a large range of projects.

**James D. Widmer** is responsible for Newcastle University's 'Centre for Advanced Electrical Drives'. Part of the University's Power Electronics, Drives and Machines Research group, the Centre works with numerous Industry partners to convert academic research into world class products. James' research interests include rare-earth magnet free motor topologies for the automotive industry, including Switched Reluctance and other Motor types, as well as including research into high performance and high efficiency Permanent Magnet machines. James joined Newcastle University in 2009 from a senior post in the Aerospace Industry.